

Network reconstruction from infection cascades

Alfredo Braunstein*

*DISAT, Politecnico di Torino, Corso Duca Degli Abruzzi 24, 10129 Torino
Human Genetics Foundation, Via Nizza 52, 10124 Torino and
Collegio Carlo Alberto, Via Real Collegio 1, Moncalieri*

Alessandro Ingrosso†

Center for Theoretical Neuroscience, Columbia University, New York, USA

Reconstructing propagation networks from observations is a fundamental inverse problem, and it's crucial to understand and control dynamics in complex systems. Here we show that it is possible to reconstruct the whole structure of an interaction network and to simultaneously infer the complete time course of activation spreading, relying just on single snapshots of a small number of activity cascades. The method, that we called Inverse Dynamics Network Reconstruction (IDNR), is shown to work successfully on several synthetic and real networks, inferring the networks and the sources of infection based on sparse observations, including single snapshots. IDNR is built on a Belief Propagation approximation, that has an impressive performance in a wide variety of topological structures. The method can be applied in absence of complete time-series data by providing a detailed modeling of the posterior distribution of trajectories conditioned to the observations. Furthermore, we show by experiments that the information content of full cascades is relatively smaller than that of sparse observations or single snapshots.

Much effort has been devoted recently to the inverse problem of reconstructing the structure of a network from time series of activity propagation. The methods proposed so far in the literature heavily rely on complete knowledge of the dynamical trajectories of some spreading process. In certain cases, when information about the time-series of the process is available, the problem can be, and has been, cast into relatively simple terms, since a sequence of time-consecutive states of a pair of nodes gives direct information about the potential interaction between them. In many cases, however, the set of available observations is much sparser, possibly on a much slower timescale than that of the dynamics, and often skipping the initial stages of the propagation which would give precious information about the source. In particular, in a single snapshot of the system there is no *direct* information about the interaction of nodes, as evidence of interaction indeed comes from variation of the state of nodes in time.

Let us take the example of second messenger cascades in a cell, and suppose the experimenter has access to the expression profile of a huge number of proteins in different cascades. Monitoring the exact time course of the concentration of each protein is currently challenging, if not unfeasible: one observes a concerted up and down-regulation of a big number of proteins, which naturally follow from a complex time course in a network of reciprocal protein-protein interactions. One is confronted with a similar information shortage in the context of epidemic spreading in a network of individuals: there's no information about who was the first one to contract the disease, and little is known about the underlying networks of contacts between individuals, which may even be dynamically changing over time.

Even though direct experimental data about contact networks in diverse contexts is being collected at a fast rate [1–3], there are some strong limitations to this collection, be them experimental, technical, or even due to privacy concerns. The knowledge of propagation networks would have a large list of benefits. First, it may allow to understand the propagation process better, including finding the entry-point (the so called *patient zero* in epidemiological jargon). Second, it may allow to devise strategies to control the process in various ways, for example hindering the propagation (e.g. targeted vaccination) or favoring it (e.g. in the context of maximizing information diffusion on social networks, in viral or targeted advertising, etc). Recently, several approaches have been proposed for the problem of deducing the propagation network from time-series, based on a naive Bayes approach [4] with efficient computations based on dynamic message-passing equations [5, 6], or on compressed sensing schemes [7]. These methods all share the need for observations at consecutive epochs.

Despite this recent progress, in most contexts the available observations of each cascade are sparse, noisy and discontinuous in time. In such situations, none of the methods proposed in the literature can be applied. One example is the problem of inferring functional contacts in signaling pathways, in which interacting proteins generate cascades of phosphorylation which eventually transmit signals from the cell membrane to the nucleus. Observations come in general from gene expression data, and the network to be inferred is a subnetwork of a large scale protein-protein interaction network (PPI). Social science and epidemiology offer another interesting domain of application, as

* alfredo.braunstein@polito.it

† ai2367@cumc.columbia.edu

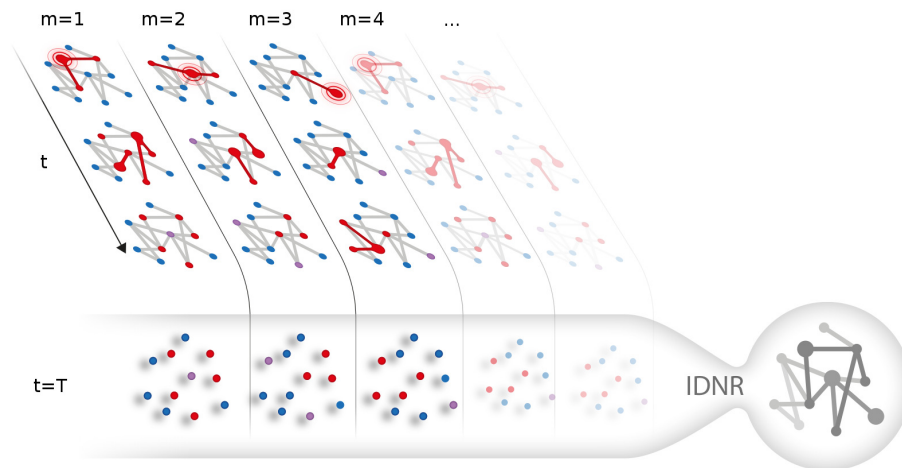


Figure 1. Cartoon representation of the Inverse Dynamics Network Reconstruction problem: M independent cascades starting from different sources (highlighted in the first frame of each vertical stripe) are represented, with time flowing downward. Infected nodes are red, Susceptible nodes are blue and Recovered nodes are purple. The IDNR algorithm is provided a set of M snapshots taken T time steps after the cascade onset: the goal is to reconstruct the functional interactions in the network G as well as to identify the source of each cascade.

one generally tries to infer the network of social contacts from a limited amount of sparse and noisy observations of some propagation histories.

Here we present a Bayesian technique that allows to uncover the complete functional structure of a network from a limited amount of single snapshots of the state of the network cascades. Starting from a functional parametrization of the posterior probability distribution of propagation trajectories, our technique builds on a Message Passing procedure that allows to compute, and then maximize, the likelihood of a given network structure. This computation can be performed efficiently thanks to Belief Propagation (BP), which is proven to be exact for tree graphs and has been successfully used in a variety of problems in general graphs with loops. Upon convergence, the parameters allow both to identify the network and the sources of the infection for each cascade with great accuracy. The method is effective on progressive propagation models like susceptible-infected (SI), susceptible-infected-removed (SIR), independent cascades (IC) and variants, including models with hidden variables (e.g. representing latency times). We called this method Inverse Dynamics Network Reconstruction (IDNR).

Although the proposed inference machinery is very general, we focus on the well known Susceptible-Infected-Recovered (SIR)[8] model, which describes those diseases in which infected individuals become immune to future infections after recovery (such as measles, rubella, chicken pox and generic influenza). More generally, SIR constitutes a good model for the spreading of rumor and information over a network.

Our minimal model of activity propagation in a network is very simple: if a node i is active (Infected) at time t , it has a finite probability λ_{ij} to activate (or infect) any of its neighbors j , which will in turn be active at time $t + 1$. An active node will recover in each time step with a (generally site-dependent) recovery probability μ_i . Once recovered, individuals do not get sick anymore, and won't be able to infect other nodes. This will result in a propagation throughout the network, that we call a cascade.

Let us then suppose that a number M of independent realizations (or cascades) of the SIR dynamics can be observed but only a limited information is available for each of them. In the prototypical situation, the complete history of the propagation is not available: all we can observe is a number of “frozen” snapshots of a wave-front of the activity at a given time T , when all the states of the nodes in the network can be assessed to a reasonable extent of accuracy. Our aim is to identify the hidden network structure and the set of transmission probabilities for each link. Fig. 1 shows a cartoon representation of the problem.

RESULTS

A static formulation of the dynamical process

Reconstructing the unknown connectivity structure of the network is inevitably coupled to that of tracing back in time the entire history of the spreading process for each cascade m , $m \in \{1, \dots, M\}$, which in turn results in the identification of the sources of diffusion. Our approach builds on computing a joint posterior probability distribution over all the cascades compatible with the observations, and then maximizing the likelihood of interaction parameters of the network at the same time. To set our notation, let us consider a weighted undirected graph $G = (V, E, \Lambda, \Omega)$ with a number $|G|$ of nodes, where $\Lambda = \{\lambda_{ij}\}_{ij \in E}$ play the role of edge-dependent infection probabilities in a SIR stochastic model, and that is also equipped with a set $\Omega = \{\mu_i\}_{i \in V}$ of site-dependent recovery probabilities. Focusing, for the moment, on a single cascade, at any point in time each node i will be in one of three possible states: susceptible (S), infected (I), and recovered/removed (R). The state of node i at time t in each cascade m is represented by a variable $x_i(t) \in \{S, I, R\}$, with t in some discrete set. At each time step (e.g. a day) of the stochastic dynamics, an infected node i can first spread the disease to each susceptible neighbor j with given probability λ_{ij} , then recover with probability μ_i . Each cascade is defined by the set of vectors $\mathbf{x}^m(t)$, with m labeling the cascade, and we assume that for each cascade the initial state $\mathbf{x}^m(0)$ is composed of just one Infected node i_0^m , with all the other nodes in the network in the being in the Susceptible state. We will assume that we have access to the state of the nodes in the networks only $T^m = T$ steps after the initiation of each cascade.

Let us consider a node i which gets infected at its infection time t_i : since it has a finite probability to pass the disease to a neighbor j in each time step, this results in a stochastic transmission delay s_{ij} . In addition, the individual i recovers at time $t_i + g_i$, with g_i a stochastic recovery delay. Owing to the irreversibility of the spreading process, each cascade is fully specified by the quantities $\{t_i, g_i\}_{i \in V}$ and $\{s_{ij}\}_{(i,j) \in E}$ for each node and each link in the network. It is then possible to construct a simple static graphical model representation of the dynamical process for each cascade on the grounds of the following simple observation: the time at which a given node i gets infected only depends on the infection times of its neighbors j , and the infection delays of these nodes. Infection times are related by the deterministic equations

$$t_i = 1 + \min_{j \in \partial i} \{t_j + s_{ji}\} \quad (1)$$

which are a set of $|G|$ constraints encoding the infection dynamics, involving only local quantities at each node. Once the stochastic quantities s_{ij} and g_i are thrown independently at random, the infection times are given deterministically by virtue of equation (1).

This observation was exploited in a series of works [9–11] to develop a fully Bayesian method for approximating the whole probability distribution of the time evolution of the system, conditioned on some observations, and was originally used to identify the origin of the epidemic outbreak in SIR and similar models. The method is built on a Belief Propagation approximation (see Methods), which is exact on tree graphs and has proven successful in general networks with loops.

What if the underlying network is unknown, and so are the epidemic parameters $\{\lambda_{ij}, \mu_i\}$? In a Maximum Likelihood approach, one needs to define the quantity $\mathcal{P}(\{\mathbf{x}^m(T)\} | \{\lambda_{ij}\}, \{\mu_i\})$, namely the likelihood of epidemic parameters with respect to observations, and then be able to maximize over the relevant parameters. In a fully Bayesian framework, incorporation *a priori* information on the network topology or epidemic parameters is straightforward: it would lead to the introduction of a term $f_{\lambda, \mu} = \log \mathcal{P}_{\lambda}(\{\lambda_{ij}\}) + \log \mathcal{P}_{\mu}(\{\mu_i\})$ in the log-likelihood, serving as a prior. The log-likelihood of the parameters is nothing but the so-called free-entropy of the system $\mathcal{L}(\{\lambda_{ij}\}, \{\mu_i\}) = \log \mathcal{P}(\{\mathbf{x}^m(T)\} | \{\lambda_{ij}\}, \{\mu_i\}) = -f(\{\lambda_{ij}\}, \{\mu_i\})$, which can be computed, consistently with the BP approximation, employing the Bethe decomposition (see Methods).

The BP method for the (cavity) marginal distributions of infection times can be then interleaved with simple log-likelihood climbing steps in a Gradient Ascent (GA) scheme, leading to a unique set of equations that are solved by iteration. In this setting, the computation of the gradient of the log-likelihood relies only on local updates involving the BP cavity messages. Ultimately all the information has to be processed locally at each node. That, in addition to other simplifications, entails a huge reduction of computational time, making the analysis of large-scale networks attainable (see Methods). One starts from a flat assignment of the parameters, and the initial fully connected network gets progressively pruned by means of the GA updates, eventually leading to a reconstructed network strongly resembling the real one.

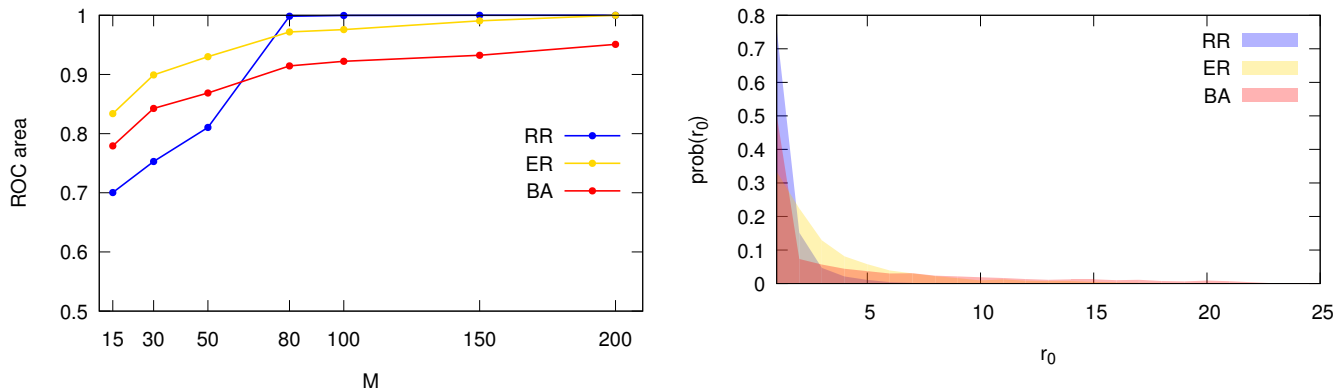


Figure 2. Left: Reconstruction accuracy in three types of random networks. Each curve is an average over 30 random instances of the area under the *ROC* curve, as a function of the number of observed cascades M at time $T = 5$. Epidemic parameters, $\lambda_{ij} = 0.6$ and $\mu_i = 0.4$, are the same for all the three type of networks. The size of the network is $|G| = 50$. Blue curve (RR): Random Regular graphs with degree $d = 4$; red curve (BA): Barabasi-Albert (scale-free) networks with average degree $d_{av} = 4$; yellow curve (ER): Erdos-Renyi graphs with average degree $d_{av} = 4$. Right: Identification of initial spreaders. Each filled curve is the histogram of the rank of the true patient zero i_0^m at $M = 150$ for the three types of network. Histograms refers to 30 random instances, thus considering a total of $30 * 150 = 4500$ independent cascades.

Reconstructing random networks

We start by investigating three basic random network structures, namely Random Regular (RR), Erdos-Renyi (ER) and Barabasi-Albert (BA) scale-free networks: an impressive level of accuracy may be reached with a small number M of observations. In a RR network, each node is connected at random with a fixed number of neighbors in the networks, whereas in the ER graph the number of neighbors is Poisson distributed. Scale-free networks, on the other hand, possess a power law degree distribution, and are known to capture some key ingredients of many real networks encountered in practical applications (for a review, see [12]).

As a first step, a random graph is constructed, and a set of M cascades are simulated, each one being an independent realization of the stochastic SIR process with a random initial source i_0^m . IDNR is then run until the parameters λ_{ij} and μ_i reach a stable value. Since the goal of the inference is two-fold, we use two different measures of the inference performance. For each cascade m , the nodes in the network are ranked in decreasing order with respect to the estimated probability of being the origin of the observed epidemics: the ability to identify the sources of the spreading is easily quantified by the rank of i_0^m , namely the position of i_0^m in the ordered list, averaged over the single cascades and, possibly, over different instances of the random graphs.

On the other hand, a simple method for quantifying the accuracy of network reconstruction is the *Receiver Operating Characteristic (ROC)* curve, namely a plot of the *true positive rate* against the *false positive rate* in a binary classification problem. Constructing the *ROC* curve in the present case is very easy: the values of λ_{ij} are ranked in decreasing order, and one step upward in the *ROC* is taken if the link is present in the original graph (true positive) or one step rightward if the link is non present (false positive). The area under the *ROC* curve is a good indication of the discrimination ability, areas close to one signaling a good discrimination between true links and non-existent links. We report in 2 (Left) a systematic investigation of the reconstruction performance in the three types of random networks with an increasing number of cascades M .

The ability to identify the sources of spreading (patient zero) is easily quantified by the rank $r_0^{(m)}$ of the true patient zero i_0^m in each of the M cascades: if M is high enough so that enough information is conveyed on the underlying network structure, IDNR is able to successfully identify most of the true initial spreaders in each cascade. This is exemplified in Fig. 2 (Right), where we show the histograms of the ranks for a value of $M = 150$ in the three types of random networks considered here.

As can be seen in Fig. 3 (Left), the distribution of inferred true links rapidly separates from the one of non-existent links, that concentrates around vanishing values even for a very small number of observations. The strict separation of the two distributions confirms the results from the area under the *ROC* curve.

It is worth noting that IDNR achieves a good level of reconstruction accuracy in a very small number of steps. The dynamics of the inferred λ_{ij} as a function of iterations of the algorithm is exemplified in Fig. 3 (Right). Even after a very small number of iterations, true links are clearly distinguished from non-existent ones, as can be seen from the steep rise of the area under the *ROC* curve as a function of iterations: we observe that this kind of behavior is quite

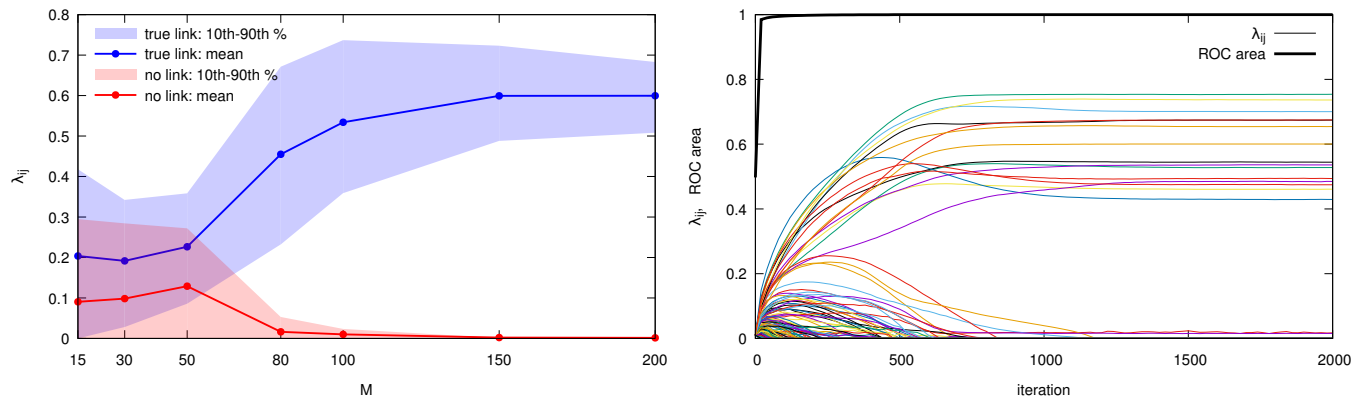


Figure 3. IDNR rapidly identifies true links. Left: average value of λ_{ij} for true links (blue) versus non-existent ones (red) as a function of the number of observed cascades in a Random Regular graph with size $|G| = 50$, $\lambda_{ij} = 0.6$, $\mu_i = 0.4$; shaded areas correspond to the intervals between the 10th and the 90th percentile in each distribution. Right: the thin lines represent the λ_{ij} values of a random subset of 200 links in the case with $M = 200$ cascades as a function of iterations of the IDNR algorithm; black thick line: area under the *ROC* curve.

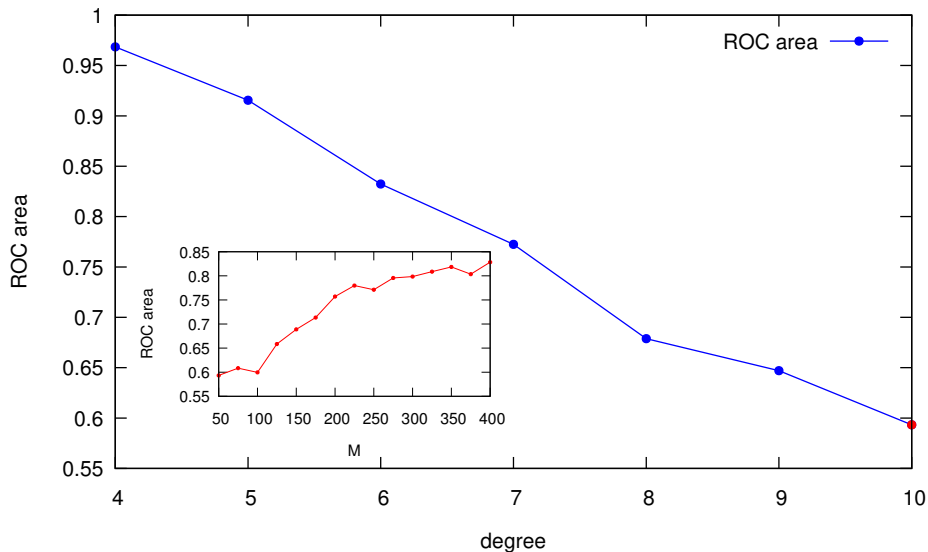


Figure 4. Reconstruction accuracy versus connectivity in random regular graphs. The blue curve is the area under the *ROC* curve in different instances of Random Regular graphs of size $|G| = 50$ with increasing degree d . In each case, $M = 50$ cascades are observed at time $T = 7$. Recovery rate is fixed to $\mu_i = 0.4$, λ_{ij} is scaled down as degree increases in order to keep the size of epidemics roughly constant. *Inset*: area under the *ROC* curve as a function of the number of observed cascades M in a random regular graph with degree $d = 10$ (corresponding to the red point at the end of the blue curve in the main plot).

general and not restricted to the case $M = \mathcal{O}(N)$.

The reconstruction performance is expected to be substantially related to the density of the network. This can be investigated by systematically varying the degree of connectivity of a network, as it is shown in Fig. 4, where the performance of IDNR is assessed in a RR graph of size $|G| = 50$ with an increasing connectivity degree d , from $d = 4$ to $d = 10$. The accurate reconstruction of denser networks requires, consequently, a bigger number of cascades M .

Reconstructing real networks

We tested the IDNR algorithm on several instances of real interaction networks. The first dataset consists of a network of Twitter retweets [13, 14]: the network is composed of $|G| = 96$ nodes, which represent Twitter users, linked through $|E| = 117$ edges corresponding to retweets (these were collected from various social and political

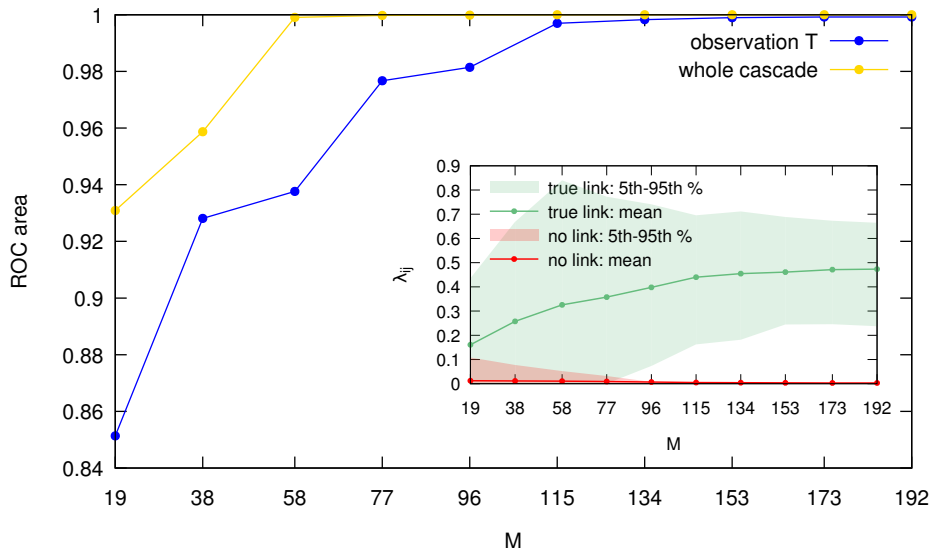


Figure 5. Reconstruction performance of IDNR in the network of retweets ($|G| = 96$) with increasing number of independent cascades M . Epidemic parameters are $\lambda_{ij} = 0.5$ and $\mu_i = 0.4$, observation time $T = 5$. Gold curve: area under ROC curve in the case where the state of the networks is fully observed at each time for each cascade m . Blue curve: area under ROC curve in the case where the network is observed only at time T in each cascade. *Inset*: average value of λ_{ij} for true links (green) versus non existent ones (red) as a function of the number of observed cascades in the standard case (observation at time T only); shaded areas correspond to the intervals between the 5th and the 95th percentile in each distribution.

hash-tags). The average degree of a node in the network is $d_{av} = 2$, with a minimum degree of 1 and a maximum degree of 17. Figure 5 shows the reconstruction performance in the retweet networks using two different observation paradigms: in the single-observation-per-cascade paradigm (which we considered as the standard case), the network state is available only once per cascade, whereas in the whole-cascade paradigm all the nodes are observable at any time. It is apparent that an extremely accurate reconstruction is achievable with a number of cascade M quite small compared to $|G|$.

As another illustrative example, in Fig. 6 we show a pictorial representation of the reconstruction of the famous Zachary’s Karate Club network, a small social network which consists of $|G| = 34$ nodes and $|E| = 78$ edges, documenting the pairwise interactions over the course of three years among members of an university-based karate club. In this case, we simulated up to $M = 102$ cascades and investigated the performance of the inference method with homogeneous parameters $\lambda = 0.3$ and $\mu = 0.4$ at increasing M . In Fig. 6, links not present in the actual graph are colored in red, and appear clearly distinguished from the true ones (colored in black) even for very small values of M .

For a more thorough representation of the reconstruction process in the Karate Club network, we show in Fig. 7 (Left) a color intensity plot of the dynamics of inference as the number of cascades is increased: true links are immediately identified, as the ROC area indicates (Right, blue curve).

It is very interesting to note that, while observing cascades in their entirety clearly conveys a lot of information on the network structure, if the total number of observations of the full state of the network is constrained, distributing these observations far apart in time pays better. This is clearly shown in Fig. 7 (Right) by the difference in the area under the ROC curve between the whole cascade scenario and the single-observation-per-cascade paradigm.

Inferring transmission probabilities

Let us now briefly consider a slightly different application of the general formalism presented so far. Suppose that the underlying network structure is known but little or any information is available on the transmission probabilities λ_{ij} , which are, in the general case, inhomogeneous. Our method can be easily accommodated so as to provide the maximum likelihood estimation of the quantities λ_{ij} . There is no need to prune a fully connected network, so that one starts with a flat assignments of the coupling parameters defined over a known network, and waits for the coupled BP-GA algorithm to reach a fixed point.

As an example, we consider a random regular graph of size $|G| = 20$ with degree $d = 4$, and evaluate the inference

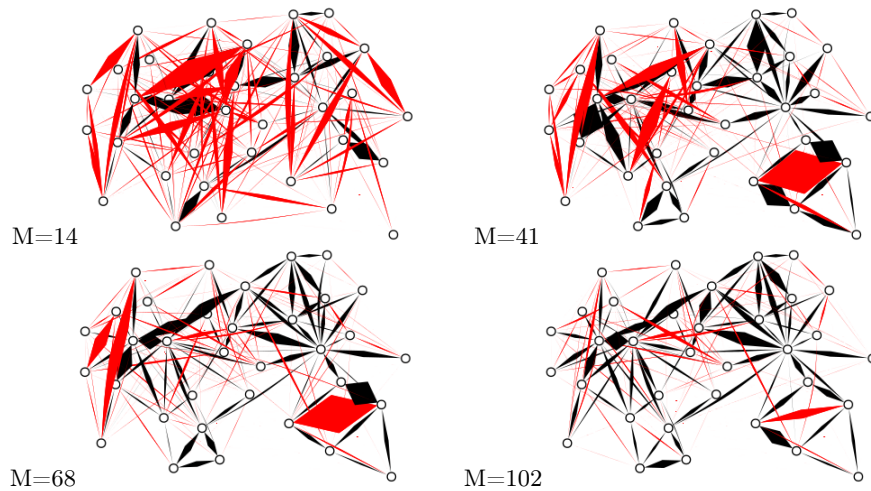


Figure 6. Pictorial representation of the IDNR performance in Zachary's Karate Club network with an increasing number of cascades M . An edge is thrown between node i and node j if λ_{ij} is non zero, the width of the edge being proportional to the value λ_{ij} . True links are colored in black, red links are not present in the original network.

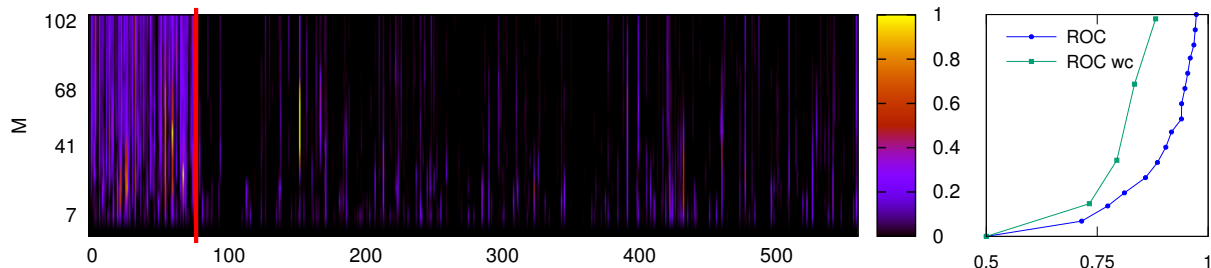


Figure 7. Left: Reconstruction performance of IDNR in the Zachary's Karate Club network with different numbers M of independent cascades. M is on the y axis. The links are on the x axis, ordered in such a way that the first 78 are the true links in the original graph. The color intensity is proportional to the value λ_{ij} for each putative link (i, j) at increasing values of M . Right: area under the ROC curve (x axis) for increasing total observations (see text) of the entire networks (y axis, scale as in the left part). The red curve corresponds to a single final observations per cascade at time $T = 5$, the green curve shows the case in which cascades are fully observed.

performance with increasing number of cascades M . Figure 8 (Left) shows the value of the Mean Square Error $MSE = \frac{\sum_{i < j} (\lambda_{ij} - \lambda_{ij}^{true})^2}{|E|}$ between the inferred transmission probabilities λ_{ij} and the true ones, λ_{ij}^{true} . To better appreciate the quality of the inference, we show a scatter plot for two different values of M in Figure 8 (Right).

DISCUSSION

We have presented a new method that enables to reconstruct a hidden network from extremely limited information of activity propagations, and showed that the reconstruction performance is extremely accurate even when the number of snapshot observations is very small.

There are several advantages of this approach over existing ones. The main one is that several inference problems can be treated under a unique formulation. Our technique can be easily extended to incorporate effects of unreliable observations, taking into account all those situations when some noise enters the measurements, or all those cases where Susceptible nodes cannot be distinguished from Recovered ones [11]. When a complete list of contact times between nodes is available, the construction of an equivalent network of timely dependent infection probability is straightforward, and the current approach has been proven to be effective. In passing, let us point out that we recently devised an efficient method for performing inverse dynamics on timely defined networks, when these types of data are actually available [15].

Owing to the generality of the Bayesian method, our technique is capable of dealing with a wide variety of irreversible

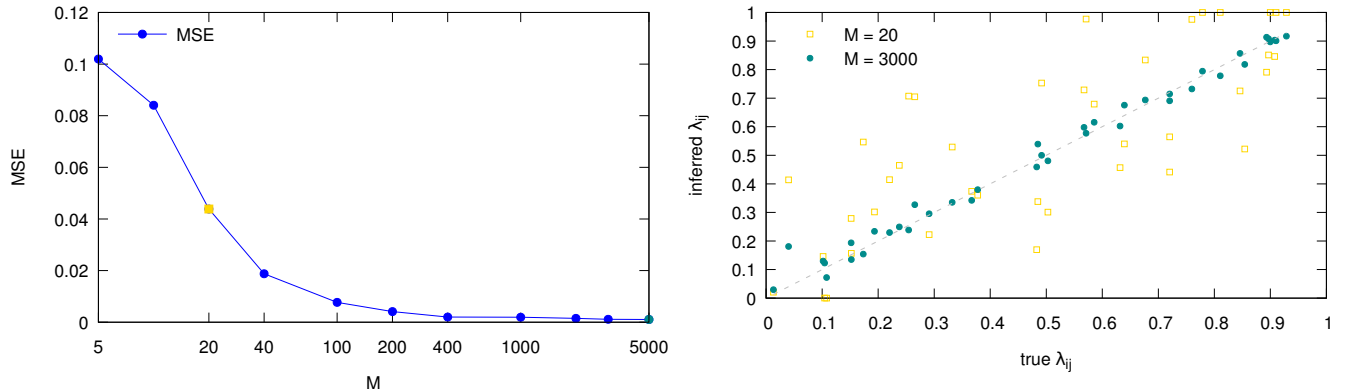


Figure 8. Reconstructing spreading couplings in inhomogeneous networks. Left: mean squared reconstruction error $MSE = \frac{\sum_{i < j} (\lambda_{ij} - \lambda_{ij}^{true})^2}{|E|}$ in a random regular graph of size $|G| = 20$ and degree $d = 4$, as a function of the number of observed cascades M . The network structure is known in advance. The spreading couplings λ_{ij}^{true} have been extracted randomly from the homogeneous distribution in the interval $[0, 1]$. The state of the network is observed only at time $T = 5$ for each cascade. Right: scatter plot of reconstructed transmission probabilities λ_{ij} versus true spreading couplings λ_{ij}^{true} for the cases $M = 20$ and $M = 3000$, corresponding to the golden and green points in the left plot, respectively.

spreading processes on networks. The simplest generalization is the (random) Bootstrap Percolation case where each node possesses an intrinsic stochastic activation threshold, so that it gets activated only when it receives inputs from a given (in general site-dependent) number of neighbors. These models are widely used to describe the features of dynamical processes in neuronal networks.

METHODS

Graphical model formulation of the spreading process

Let us first consider a single cascade on a network with a fixed topology. For a fixed initial configuration $\mathbf{x}(0)$, a realization of the stochastic process can be generated by drawing randomly a set of infection transmission delay s_{ij} for all pairs (ij) and the recovery times g_i of each node i . The recovery times $\{g_i\}$ are independent random variables extracted from the geometric distributions $\mathcal{G}_i(g_i) = \mu_i (1 - \mu_i)^{g_i}$, the delays $\{s_{ij}\}$ are conditionally independent random variables distributed according to a truncated geometric distribution,

$$\omega_{ij}(s_{ij}|g_i) = \begin{cases} \lambda_{ij} (1 - \lambda_{ij})^{s_{ij}}, & s_{ij} \leq g_i \\ \sum_{s > g_i} \lambda_{ij} (1 - \lambda_{ij})^s, & s_{ij} = \infty, \end{cases}$$

Note that we concentrate in the value $s_{ij} = \infty$ the mass of the distribution beyond the hard cut-off g_i imposed by the recovery time. The joint probability distribution of infection and recovery times conditioned on the initial state is easily written:

$$\begin{aligned} \mathcal{P}(\mathbf{t}, \mathbf{g} | \mathbf{x}(0)) &= \sum_{\mathbf{s}} \mathcal{P}(\mathbf{s} | \mathbf{g}) \mathcal{P}(\mathbf{t} | \mathbf{x}(0), \mathbf{g}, \mathbf{s}) \mathcal{P}(\mathbf{g}) \\ &= \sum_{\mathbf{s}} \prod_{i,j} \omega_{ij}(s_{ij}|g_i) \prod_i \psi_i(t_i, \{t_k, s_{ki}\}_{k \in \partial i}) \mathcal{G}_i(g_i), \end{aligned} \quad (2)$$

where

$$\psi_i(t_i, \{t_k, s_{ki}\}_{k \in \partial i}) = \delta(t_i, \mathbb{I}[x_i(0) \neq I](1 + \min_{k \in \partial i} \{t_k + s_{ki}\})) \quad (3)$$

is a characteristic function which imposes on each node i the dynamical constraint of equation (1).

Using the Bayes formula, and incorporating a prior $\mathcal{P}(\mathbf{x}(0))$ of the initial state of the network, the posterior probability of the initial configuration given an observation at time T reads:

$$\mathcal{P}(\mathbf{x}(0) | \mathbf{x}(T)) \propto \sum_{\mathbf{t}, \mathbf{g}} \mathcal{P}(\mathbf{x}(T) | \mathbf{t}, \mathbf{g}) \mathcal{P}(\mathbf{t}, \mathbf{g} | \mathbf{x}(0)) \mathcal{P}(\mathbf{x}(0)) \quad (4)$$

$$= \sum_{\mathbf{t}, \mathbf{g}, \mathbf{s}} \prod_{i,j} \omega_{ij} \prod_i \psi_i \mathcal{G}_i \gamma_i \zeta_i^T \zeta_i^0 \quad (5)$$

where $\mathcal{P}(\mathbf{x}(0)) = \prod_i \gamma_i(x_i(0))$ is a factorized prior on the initial infection with

$$\gamma_i(x_i(0)) = \gamma \delta(x_i(0), I) + (1 - \gamma) \delta(x_i(0), S) \quad (6)$$

for a generally small constant γ . Note that the network state $\mathbf{x}(t)$ is a deterministic function of the set of infection and recovery times (\mathbf{t}, \mathbf{g}) , so that we obtain

$$\mathcal{P}(\mathbf{x}(T) | \mathbf{t}, \mathbf{g}) = \prod_i \zeta_i^T(t_i, g_i, x_i(T)) \quad (7)$$

$$\mathcal{P}(\mathbf{t}, \mathbf{g} | \mathbf{x}(0)) \propto \prod_i \zeta_i^0(t_i, g_i, x_i(0)) \quad (8)$$

with

$$\zeta_i^t = \mathbb{I}[x_i(t) = S, t < t_i] + \mathbb{I}[x_i(t) = I, t_i \leq t < t_i + g_i] + \mathbb{I}[x_i(t) = R, t_i + g_i \leq t]. \quad (9)$$

Now, if we introduce a set of observational weights $\zeta_i^{m,T}$, one for each observation m , together with a set of priors $\zeta_i^{m,0}$, the full distribution, because of the assumption of independence, will just be the product over all the single probability weights for each cascade as in equation (5) and will take the form:

$$\begin{aligned} \mathcal{P}(\{\mathbf{x}^m(0)\} | \{\mathbf{x}^m(T)\}) &\propto \prod_{m=1}^M \sum_{\mathbf{t}^m, \mathbf{g}^m} \mathcal{P}(\mathbf{x}^m(T) | \mathbf{t}^m, \mathbf{g}^m) \mathcal{P}(\mathbf{t}^m, \mathbf{g}^m | \mathbf{x}^m(0)) \mathcal{P}(\mathbf{x}^m(0)) \\ &= \prod_{n=1}^M \sum_{\mathbf{t}^m, \mathbf{g}^m, \mathbf{s}^m} \prod_{i,j} \omega_{ij}^m \prod_i \psi_i^m \mathcal{G}_i^m \gamma_i^m \zeta_i^{m,T} \zeta_i^{m,0} \end{aligned} \quad (10)$$

where all the factors have been labeled with an extra cascade index m . Since we have no a priori information on the graph topology, the product in the term $\prod_{i,j} \omega_{ij}^m$ runs over all the possible pair i and j in the set V , meaning that we always work in the setting of a fully connected network with weights $\{\lambda_{ij}\}$. If the number of cascades M is large enough, the non zero elements of the matrix $\{\lambda_{ij}\}$ will signal, upon convergence of the IDNR algorithm, the true links in the original graph, their value being informative of the heterogeneity of infection probabilities. The same holds for the set of recovery parameters $\{\mu_i\}$.

Belief Propagation approach

Given a high dimensional probability distribution $M(\mathbf{z})$ with a locally factorized interaction structure, computing marginals and aggregated quantities may be addressed with the use of a Message Passing procedure built on a cavity approximation for locally tree-like graphs [16–18]. In the present problem, we obtain a full set of (cavity) marginal probabilities over the set of all the possible cascades compatible with the observations. BP is proven to be exact on tree graphs, and has been successfully employed on general loopy graphs under mild regularity conditions[9, 19][9, 19].

To briefly describe the essence of the the method, let us consider a probability distribution over the variables $\mathbf{z} = \{z_i\}$ that has the following factorized form:

$$M(\mathbf{z}) = \frac{1}{Z} \prod_a \chi_a(\mathbf{z}_a) \quad (11)$$

where each χ_a is called compatibility function, or *factor*. We write $\mathbf{z}_a = \{z_i\}_{i \in \partial a}$ as the set of variables it depends on, ∂a the subset of indices of variables in factor χ_a , and accordingly ∂i will be the subset of factors that depend on z_i .

Belief Propagation equations are a set of self-consistent equations for the so-called *cavity messages* (or *beliefs*), a set of single-site probability distributions which are associated to each directed link in the graphical model representing to the joint distribution of equation (11). The general form of BP equations is the following:

$$p_{\chi_a \rightarrow i}(z_i) = \frac{1}{Z_{ai}} \sum_{\{z_j: j \in \partial a \setminus i\}} \chi_a(\mathbf{z}_a) \prod_{j \in \partial a \setminus i} m_{j \rightarrow \chi_a}(z_j) \quad (12)$$

$$m_{i \rightarrow \chi_a}(z_i) = \frac{1}{Z_{ia}} \prod_{b \in \partial i \setminus a} p_{\chi_b \rightarrow i}(z_i) \quad (13)$$

$$m_i(z_i) = \frac{1}{Z_i} \prod_{b \in \partial i} p_{\chi_b \rightarrow i}(z_i) \quad (14)$$

where the terms Z_{ia} , Z_{ai} and Z_i are local partition function, serving as normalizers. To solve equations (12) and (13) an iterative procedure is typically used, where the cavity messages are initialized with homogeneous distributions and they are asynchronously updated until convergence to a fixed point (see e.g. [16, 18] for an introduction). The BP equations can be thought as local update rules for messages in a so-called Factor Graph, a bipartite graph where each term χ_a is associated to a factor node, connected to all the variable nodes in the set \mathbf{z}_a it depends on. A naive implementation of the BP scheme at the level of equation (10) would simply not work, since the corresponding graphical model has a loopy structure both at local and global scale. It is although possible to construct a disentangled factor graph by means of a re-parametrization of the cavity messages. We provide a brief description of this procedure in the Supplementary Methods. For a thorough discussion we refer the reader to previous works (see [10], [11]). Here we just want to stress that the modified factor graph is an enriched dual version of the original graph, whence the particular appeal of the method. In particular, this implies that Belief Propagation provides the exact Bayesian solution when the underlying network is a tree.

While the computation of equation (13) is straightforward, the sum in equation (12) generally involves a number of steps growing exponentially with the size of ∂a . An efficient implementation of the BP equations for the posterior distribution is given in the Supplementary Methods. Once Belief Propagation converges, equation (14) can be used to compute the marginal probability $\mathcal{P}(t_i^n = 0 \mid \{\mathbf{x}^m(T)\})$, which brings a posterior estimation of the probability for the node i to be the active at time $t = 0$ in the m th cascade.

Network reconstruction algorithm

We employ an alternating optimization scheme in which Belief Propagation is coupled to a Maximum Likelihood strategy, implemented with a Gradient Ascent method. In the BP phase, the network parameters $\{\lambda_{ij}, \mu_i\}$ are kept fixed and a solution is searched iteratively for equations (12) and (13). At this stage, the source can be located independently for each cascade looking at the single-site marginals $\mathcal{P}(x_i^m(0) \mid \{\mathbf{x}^m(T)\})$. In the Maximum Likelihood phase, the log-likelihood of network parameters is maximized by means of a simple Gradient Ascent (GA) procedure. The gradient may be computed efficiently in the BP approximation. The likelihood with respect to the network parameters is defined as

$$\mathcal{P}(\{\mathbf{x}^m(T)\} \mid \{\lambda_{ij}\}, \{\mu_i\}) = \prod_{m=1}^M \sum_{\mathbf{t}^m, \mathbf{g}^m} \mathcal{P}(\mathbf{x}^m(T) \mid \mathbf{t}^m, \mathbf{g}^m) \mathcal{P}(\mathbf{t}^m, \mathbf{g}^m \mid \mathbf{x}^m(0)) \mathcal{P}(\mathbf{x}^m(0)) = Z(\{\lambda_{ij}\}, \{\mu_i\})$$

The logarithm of this quantity (log-likelihood) corresponds to the negative free energy of the model $\mathcal{L}(\{\lambda_{ij}\}, \{\mu_i\}) = -f(\{\lambda_{ij}\}, \{\mu_i\}) = \log Z(\{\lambda_{ij}\}, \{\mu_i\})$, and can be expressed as a sum of local terms depending only on the BP messages (see Supplementary Methods). BP updates for the distribution in equation (10) are then coupled to Gradient Ascent (GA) updates with respect to each network parameter, that take the form:

$$\lambda_{ij} \leftarrow \lambda_{ij} + \epsilon \frac{\partial \mathcal{L}}{\partial \lambda_{ij}} \quad (15)$$

$$\mu_i \leftarrow \mu_i + \epsilon \frac{\partial \mathcal{L}}{\partial \mu_i} \quad (16)$$

with ϵ a small convergence parameter. The results presented in this work have been obtained with the simple and successful approach of simply interleaving one BP step with a GA step, without waiting for BP to converge with fixed network parameters: a simple alternation suffices to provide good joint estimates for the patient zero in each cascade, together with a remarkably good reconstruction of the underlying network.

SUPPLEMENTARY METHODS

BP equation: efficient disentagled implementation

We would like to use a factor graph representation that maintains the same topological properties of the original graph of contacts, in order to guarantee that BP is exact when the original contact graph is a tree. Following an approach developed in previous works [9, 11, 19], we proceed to disentangle the factor graph by grouping pairs of infection times (t_i, t_j) in the same variable node. For convenience, we will keep all variable nodes $\{t_i\}$ but we will also introduce for each edge (i, j) emerging from a node i a set of copies $t_i^{(j)}$ of the infection time t_i , that will be forced to take the common value t_i by including the constraint $\prod_{k \in \partial i} \delta(t_i^{(k)}, t_i)$ in an additional factor ϕ_i .

The factors ϕ_i depend on infection times and transmission delays just through the sums $t_i^{(j)} + s_{ij}$, so that it is more convenient to introduce the variables $t_{ij} = t_i^{(j)} + s_{ij}$ and express the dependencies through the pairs $(t_i^{(j)}, t_{ij})$.

Finally it is convenient to group the variable g_i with the corresponding infection times t_i in the same variable node, replace g_i and g_j by their copies $g_i^{(j)}$ and $g_j^{(i)}$ in the edge constraints $\omega_{ij}(t_{ij} - t_i^{(j)} | g_i^{(i)})$ and $\omega_{ji}(t_{ji} - t_j | g_j^{(i)})$ and impose the identity $\prod_{k \in \partial i} \delta(g_i^{(k)}, g_i)$ for each node i . The resulting disentangled factor graph appears in Fig. 9.

An efficient form for the update equations of the ψ_i factor nodes is the following:

$$p_{\psi_i \rightarrow j} \left(t_i^{(j)}, t_{ji}, g_i^{(j)} \right) \propto \sum_{g_i, t_i} \sum_{\{t_i^{(k)}, t_{ki}, g_i^{(k)}\}} m_{i \rightarrow \psi_i} (t_i, g_i) \times \quad (17)$$

$$\times \prod_{k \in \partial i \setminus j} m_{k \rightarrow \psi_i} \left(t_i^{(k)}, t_{ki}, g_i^{(k)} \right) \psi_i \left(t_i, g_i, \left\{ \left(t_i^{(k)}, t_{ki}, g_i^{(k)} \right) \right\}_{k \in \partial i} \right) \\ \propto m_{i \rightarrow \psi_i} \left(t_i^{(j)}, g_i^{(j)} \right) \sum_{t_{ki}} \prod_{k \in \partial i \setminus j} m_{k \rightarrow \psi_i} \left(t_i^{(j)}, t_{ki}, g_i^{(j)} \right) \times \quad (18)$$

$$\times \left[\delta \left(t_i^{(j)}, 0 \right) + \delta \left(t_i^{(j)}, \left(1 + \min_{k \in \partial i} \{t_{ki}\} \right) \right) \right] \\ \propto \delta \left(t_i^{(j)}, 0 \right) m_{i \rightarrow \psi_i} \left(0, g_i^{(j)} \right) \prod_{k \in \partial i \setminus j} \sum_{t_{ki}} m_{k \rightarrow \psi_i} \left(0, t_{ki}, g_i^{(j)} \right) + \quad (19)$$

$$+ m_{i \rightarrow \psi_i} \left(t_i^{(j)}, g_i^{(j)} \right) \mathbb{I} \left(t_i^{(j)} \leq t_{ji} + 1 \right) \prod_{k \in \partial i \setminus j} \sum_{t_{ki} \geq t_i^{(j)} - 1} m_{k \rightarrow \psi_i} \left(t_i^{(j)}, t_{ki}, g_i^{(j)} \right) \\ - m_{i \rightarrow \psi_i} \left(t_i^{(j)}, g_i^{(j)} \right) \mathbb{I} \left(t_i^{(j)} < t_{ji} + 1 \right) \prod_{k \in \partial i \setminus j} \sum_{t_{ki} > t_i^{(j)} - 1} m_{k \rightarrow \psi_i} \left(t_i^{(j)}, t_{ki}, g_i^{(j)} \right)$$

where in (19) we use the fact that

$$\delta \left(t_i, \left(1 + \min_{j \in \partial i} \{t_{ji}\} \right) \right) = \prod_{j \in \partial i} \mathbb{I} (t_i \leq t_{ji} + 1) - \prod_{j \in \partial i} \mathbb{I} (t_i < t_{ji} + 1).$$

Up to now, messages depend on the T^2G values $(t_i^{(k)}, t_{ki}, g_i^{(k)})$. It is though possible to use a simpler representation, retaining just information on the relative timing between infection time $t_i^{(j)}$ for a node i and the infection propagation time t_{ji} on its link with node j , introducing the variables

$$\sigma_{ji} = 1 + \text{sign} \left(t_{ji} - \left(t_i^{(j)} - 1 \right) \right), \quad (20)$$

In order to switch to the simplified representation with $(\sigma_{ji}, \sigma_{ij})$ variables defined in (20) instead of t_{ji}, t_{ij} ones, we will proceed as follows.

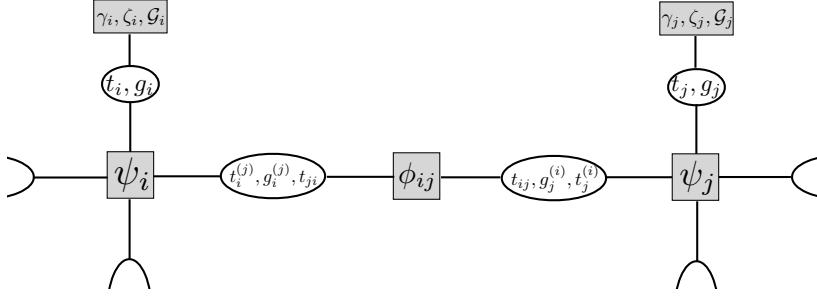


Figure 9. Disentangled Factor graph representation of the graphical model.

In equation (19) we can easily group the sums over different configurations of $(t_{ki}, t_i^{(j)})$ and write:

$$\begin{aligned}
p_{\psi_i \rightarrow j}(t_i^{(j)}, \sigma_{ji}, g_i^{(j)}) &\propto \delta(t_i^{(j)}, 0) m_{i \rightarrow \psi_i}(0, g_i^{(j)}) \prod_{k \in \partial i \setminus j} \sum_{\sigma_{ki}} m_{k \rightarrow \psi_i}(0, \sigma_{ki}, g_i^{(j)}) + \\
&+ m_{i \rightarrow \psi_i}(t_i^{(j)}, g_i^{(j)}) \mathbb{I}(\sigma_{ji} = 1, 2) \prod_{k \in \partial i \setminus j} \sum_{\sigma_{ki}=1,2} m_{k \rightarrow \psi_i}(t_i^{(j)}, \sigma_{ki}, g_i^{(j)}) \\
&- m_{i \rightarrow \psi_i}(t_i^{(j)}, g_i^{(j)}) \mathbb{I}(\sigma_{ji} = 2) \prod_{k \in \partial i \setminus j} m_{k \rightarrow \psi_i}(t_i^{(j)}, 2, g_i^{(j)})
\end{aligned} \tag{21}$$

Similarly, the outgoing message to the (t_i, g_i) variable node is:

$$\begin{aligned}
p_{\psi_i \rightarrow i}(t_i, g_i) &\propto \delta(t_i, 0) \prod_{k \in \partial i} \sum_{\sigma_{ki}} m_{k \rightarrow \psi_i}(0, \sigma_{ki}, g_i) + \\
&+ \prod_{k \in \partial i} \sum_{\sigma_{ki}=1,2} m_{k \rightarrow \psi_i}(t_i, \sigma_{ki}, g_i) \\
&- \prod_{k \in \partial i} m_{k \rightarrow \psi_i}(t_i, 2, g_i)
\end{aligned} \tag{22}$$

In the simplified (t, σ, g) representation for the messages, the update equation for the ϕ_{ij} nodes reads:

$$p_{\phi_{ij} \rightarrow j}(t_j, \sigma_{ij}, g_j) \propto \sum_{t_i, \sigma_{ji}, g_i} \Omega(t_i, t_j, \sigma_{ij}, \sigma_{ji}, g_i, g_j) m_{i \rightarrow \phi_{ij}}(t_i, \sigma_{ji}, g_i) \tag{23}$$

where:

$$\Omega(t_i, t_j, \sigma_{ij}, \sigma_{ji}, g_i, g_j) = \begin{cases} \chi(t_i, t_j, \sigma_{ij}, g_i) & : t_i < t_j, \sigma_{ji} = 2, \sigma_{ij} \neq 2 \\ \chi(t_i, t_j, \sigma_{ij}, g_i) + (1 - \lambda)^{g_i+1} & : t_i < t_j, \sigma_{ji} = 2, \sigma_{ij} = 2 \\ \chi(t_j, t_i, \sigma_{ji}, g_j) & : t_j < t_i, \sigma_{ji} = 2, \sigma_{ij} \neq 2 \\ \chi(t_j, t_i, \sigma_{ji}, g_j) + (1 - \lambda)^{g_j+1} & : t_j < t_i, \sigma_{ij} = 2, \sigma_{ji} = 2 \\ 1 & : t_i = t_j, \sigma_{ji} = \sigma_{ij} = 2 \\ 0 & : \text{otherwise} \end{cases} \tag{24}$$

and

$$\chi(t_1, t_2, \sigma, g) = \sum_{t=t_1}^{t_1+g} \delta(\sigma(t_2, t), \sigma) \lambda (1 - \lambda)^{t-t_1} \tag{25}$$

Simple algebra and precalculation of terms in (23)-(25) brings a significant optimization for updates involving the factor node ϕ_{ij} down to $O(TG^2)$ operations per update.

Gradient descent updates

The log-likelihood of the epidemic parameters is nothing but the free energy of the model. In the Bethe approximation, it can be expressed as a sum of local terms which only depends on the BP messages:

$$-f = \sum_a f_a + \sum_i f_i - \sum_{(ia)} f_{(ia)} \quad (26)$$

where

$$f_a = \log \left(\sum_{\{z_i: i \in \partial a\}} F_a(\{z_i\}_{i \in \partial a}) \prod_{i \in \partial a} m_{i \rightarrow a}(z_i) \right) \quad (27)$$

$$f_{(ia)} = \log \left(\sum_{z_i} m_{i \rightarrow a}(z_i) p_{F_a \rightarrow i}(z_i) \right) \quad (28)$$

$$f_i = \log \left(\sum_{z_i} \prod_{b \in \partial i} p_{F_b \rightarrow i}(z_i) \right) \quad (29)$$

Since f is a function of all the BP messages, one would argue that these messages depend on the model parameters too, at every step in the BP algorithm. Actually, there is no need to consider this implicit $\{\lambda_{ij}, \mu_i\}$ dependence if BP has reached its fixed point, that is when BP equations are satisfied and the messages are nothing else but Lagrange multipliers with respect to the constraint minimization of the Bethe free energy functional [16]. In the present parametrization, the only explicit dependence of free energy on epidemic parameters is in the factor node terms f_a 's involving the compatibility functions $\phi_{ij} = \omega_{ij}(t_{ij} - t_i | g_i) \omega_{ji}(t_{ji} - t_j | g_j)$ and $\mathcal{G}_i(g_i) = \mu_i(1 - \mu_i)^{g_i}$, and the gradient can be computed very easily. Please note that formulas below show the derivative of the free energy $f = -\mathcal{L}$: the GA updates of the log-likelihood only differ up to a minus sign. For the ϕ_{ij} nodes we have:

$$\frac{\partial f_{\phi_{ij}}}{\partial \lambda_{ij}} = \frac{\sum_{t_i, t_{ji}, g_i, t_j, t_{ij}, g_j} \frac{\partial \phi_{ij}}{\partial \lambda_{ij}}(t_i, t_{ji}, g_i, t_j, t_{ij}, g_j) m_{i \rightarrow \phi_{ij}}(t_i, t_{ji}, g_i) m_{j \rightarrow \phi_{ij}}(t_j, t_{ij}, g_j)}{\sum_{t_i, t_{ji}, g_i, t_j, t_{ij}, g_j} \phi_{ij}(t_i, t_{ji}, g_i, t_j, t_{ij}, g_j) m_{i \rightarrow \phi_{ij}}(t_i, t_{ji}, g_i) m_{j \rightarrow \phi_{ij}}(t_j, t_{ij}, g_j)} \quad (30)$$

where

$$\frac{\partial \phi_{ij}}{\partial \lambda_{ij}} = \begin{cases} 1 & t_i < t_j \text{ and } t_i = t_{ij} < t_i + g_i \\ -(g_i - t_i) \lambda_{ij} (1 - \lambda_{ij})^{g_i - t_i - 1} & t_i < t_j \text{ and } t_i < t_{ij} = t_i + g_i \\ (1 - \lambda_{ij})^{t_{ij} - t_i} - (t_{ij} - t_i) \lambda_{ij} (1 - \lambda_{ij})^{t_{ij} - t_i - 1} & t_i < t_j \text{ and } t_i < t_{ij} < t_i + g_i \\ 1 & t_j < t_i \text{ and } t_j = t_j < t_j + g_j \\ -(g_j - t_j) \lambda_{ij} (1 - \lambda_{ij})^{g_j - t_j - 1} & t_j < t_i \text{ and } t_j < t_{ji} = t_j + g_j \\ (1 - \lambda_{ij})^{t_{ji} - t_j} - (t_{ji} - t_j) \lambda_{ij} (1 - \lambda_{ij})^{t_{ji} - t_j - 1} & t_j < t_i \text{ and } t_j < t_{ji} < t_j + g_j \\ 0 & \text{else} \end{cases} \quad (31)$$

In the simplified (t, σ, g) representation for the messages, equation (31) takes the form:

$$\frac{\partial \phi_{ij}}{\partial \lambda_{ij}} = \begin{cases} \chi(t_i, t_j, \sigma_{ij}, g_i) & t_i < t_j, \sigma_{ji} = 2, \sigma_{ij} \neq 2 \\ \chi(t_i, t_j, \sigma_{ij}, g_i) - (g_i + 1)(1 - \lambda)^{g_i} & t_i < t_j, \sigma_{ji} = 2, \sigma_{ij} = 2 \\ \chi(t_j, t_i, \sigma_{ji}, g_j) & t_j < t_i, \sigma_{ji} = 2, \sigma_{ij} \neq 2 \\ \chi(t_j, t_i, \sigma_{ji}, g_j) - (g_j + 1)(1 - \lambda)^{g_j} & t_j < t_i, \sigma_{ji} = 2, \sigma_{ij} = 2 \\ 0 & \text{otherwise} \end{cases} \quad (32)$$

where:

$$\chi(t_1, t_2, \sigma, g) = \sum_{t=t_1}^{t_1+g} \delta(\sigma(t_2, t), \sigma) (1 - \lambda_{ij})^{t-t_1} - (t-t_1) \lambda_{ij} (1 - \lambda_{ij})^{t-t_1-1} \quad (33)$$

For the \mathcal{G}_i nodes we have:

$$\frac{\partial f_{\mathcal{G}_i}}{\partial \mu_i} = \frac{\sum_{g_i} \tilde{\mathcal{G}}_i(g_i) m_{i \rightarrow \mathcal{G}_i}(g_i)}{\sum_{g_i} \mathcal{G}_i(g_i) m_{i \rightarrow \mathcal{G}_i}(g_i)} \quad (34)$$

where

$$\tilde{G}_i(g_i) = \begin{cases} (1 - \mu_i)^{g_i} - g_i \mu_i (1 - \mu_i)^{g_i - 1} & : g_i < G \\ G - G (1 - \mu_i)^{G - 1} & : g_i = G. \end{cases} \quad (35)$$

-
- [1] Marcel Salathé, Maria Kazandjieva, Jung Woo Lee, Philip Levis, Marcus W. Feldman, and James H. Jones. A high-resolution human contact network for infectious disease transmission. *Proceedings of the National Academy of Sciences*, 107(51):22020–22025, 2010. doi:10.1073/pnas.1009094108.
- [2] Lorenzo Isella, Juliette Stehlé, Alain Barrat, Ciro Cattuto, Jean-François Pinton, and Wouter Van den Broeck. What’s in a crowd? analysis of face-to-face behavioral networks. *Journal of Theoretical Biology*, 271(1):166–180, February 2011. ISSN 0022-5193. doi:10.1016/j.jtbi.2010.11.033.
- [3] Luis E. C. Rocha, Fredrik Liljeros, and Petter Holme. Information dynamics shape the sexual networks of internet-mediated prostitution. *Proceedings of the National Academy of Sciences*, 107(13):5706–5711, March 2010. ISSN 0027-8424, 1091-6490. doi:10.1073/pnas.0914080107.
- [4] Andrey Y Lokhov and Theodor Misiakiewicz. Efficient reconstruction of transmission probabilities in a spreading process from partial observations. *arXiv preprint arXiv:1509.06893*, 2015.
- [5] Brian Karrer and M. E. J. Newman. Message passing approach for general epidemic models. *Physical Review E*, 82(1):016101, July 2010. doi:10.1103/PhysRevE.82.016101.
- [6] Andrey Y. Lokhov, Marc Mézard, Hiroki Ohta, and Lenka Zdeborová. Inferring the origin of an epidemic with a dynamic message-passing algorithm. *Phys. Rev. E*, 90:012801, Jul 2014. doi:10.1103/PhysRevE.90.012801.
- [7] Zhesi Shen, Wen-Xu Wang, Ying Fan, Zengru Di, and Ying-Cheng Lai. Reconstructing propagation networks with natural diversity and identifying hidden sources. *Nature communications*, 5, 2014.
- [8] W. O. Kermack and A. G. McKendrick. A contribution to the mathematical theory of epidemics. *Proceedings of the Royal Society of London. Series A*, 115(772):700–721, August 1927. ISSN 1364-5021, 1471-2946. doi:10.1098/rspa.1927.0118.
- [9] F. Altarelli, A. Braunstein, L. Dall’Asta, and R. Zecchina. Optimizing spread dynamics on graphs by message passing. *Journal of Statistical Mechanics: Theory and Experiment*, 2013(09):P09011, September 2013. ISSN 1742-5468. doi:10.1088/1742-5468/2013/09/P09011.
- [10] Fabrizio Altarelli, Alfredo Braunstein, Luca Dall’Asta, Alejandro Lage-Castellanos, and Riccardo Zecchina. Bayesian inference of epidemics on networks via belief propagation. *Physical Review Letters*, 112(11):118701, March 2014. doi:10.1103/PhysRevLett.112.118701.
- [11] Fabrizio Altarelli, Alfredo Braunstein, Luca Dall’Asta, Alessandro Ingrosso, and Riccardo Zecchina. The patient-zero problem with noisy observations. *Journal of Statistical Mechanics: Theory and Experiment*, 2014(10):P10016, 2014.
- [12] Réka Albert and Albert-László Barabási. Statistical mechanics of complex networks. *Rev. Mod. Phys.*, 74:47–97, Jan 2002. doi:10.1103/RevModPhys.74.47.
- [13] Ryan A. Rossi and Nesreen K. Ahmed. rt-retweet - retweet networks, 2013. URL http://networkrepository.com/rt_retweet.php.
- [14] Ryan A. Rossi and Nesreen K. Ahmed. The network data repository with interactive graph analytics and visualization. In *Proceedings of the Twenty-Ninth AAAI Conference on Artificial Intelligence*, 2015. URL <http://networkrepository.com>.
- [15] A Braunstein and A Ingrosso. Inference of causality in epidemics on temporal contact networks. *Scientific reports*, 6:27538, 2016.
- [16] Jonathan S Yedidia, William T Freeman, and Yair Weiss. Bethe free energy, kikuchi approximations, and belief propagation algorithms. *Advances in neural information processing systems*, 13, 2001.
- [17] Jonathan S. Yedidia, William T. Freeman, and Yair Weiss. Exploring artificial intelligence in the new millennium. chapter Understanding Belief Propagation and Its Generalizations, pages 239–269. Morgan Kaufmann Publishers Inc., San Francisco, CA, USA, 2003. ISBN 1-55860-811-7.
- [18] Marc Mézard and Andrea Montanari. *Information, Physics, and Computation*. Oxford University Press, January 2009. ISBN 9780198570837.
- [19] Fabrizio Altarelli, Alfredo Braunstein, Luca Dall’Asta, and Riccardo Zecchina. Large deviations of cascade processes on graphs. *Physical Review E*, 87(6):062115, June 2013. doi:10.1103/PhysRevE.87.062115.